Anderson localization of cold atomic gases with effective spin-orbit interaction in a quasiperiodic optical lattice

Lu Zhou,[1,2] Han Pu,[2] and Weiping Zhang[1]

[1]*Quantum Institute for Light and Atoms, Department of Physics, East China Normal University, Shanghai 200062, China*

[2]*Department of Physics and Astronomy and Rice Quantum Institute, Rice University, Houston, Texas 77251-1892, USA*

(Received 7 January 2013; published 25 February 2013)

We theoretically investigate the localization properties of a spin-orbit-coupled spin-1/2 particle moving in a one-dimensional quasiperiodic potential, which can be experimentally implemented using cold atoms trapped in a quasiperiodic optical lattice potential and external laser fields. We present the phase diagram in the parameter space of the disorder strength and those related to the spin-orbit coupling. The phase diagram is verified via multifractal analysis of the atomic wave functions and the numerical simulation of diffusion dynamics. We found that spin-orbit coupling can lead to spectra mixing (coexistence of extended and localized states) and the appearance of mobility edges.

DOI: 10.1103/PhysRevA.87.023625 PACS number(s): 03.75.Lm, 71.70.Ej, 72.15.Rn, 03.75.Kk

I. INTRODUCTION

Anderson localization (AL) is considered a fundamental physical phenomenon, which was first studied in the system of noninteracting electrons in a crystal with impurities [1]. AL predicts the absence of diffusion of electronic spin, which stems from the disorder of crystal and is the result of quantum interference. Since disorder is ubiquitous, AL is rather universal and can occur in a variety of other physical systems including light waves [2] and atomic matter waves [3–5]. Due to its intimate relation with metal-insulator transition, many interesting topics in AL such as the interplay between nonlinearity and disorder [6–9] are still under intense study.

In condensed-matter physics, spin-orbit (SO) coupling originates from the interaction between the intrinsic spin of an electron and the magnetic field induced by its movement. It connects the electronic spin to its orbital motion and thus the electron transport becomes spin dependent. SO interaction can significantly affect AL and this problem had been addressed by a few works in the electronic gas system [10,11].

The experimental realization of ultracold quantum gases, together with the technique of optical lattice potential, have provided a powerful playground for the simulation of condensed-matter systems. In this composite system, one can achieve unprecedented control over almost all parameters by optical or magnetic means. Specifically, pseudodisorder can be generated by superimposing two standing optical waves of incommensurate wavelengths together. As a consequence, AL of an atomic matter wave can take place, which had been experimentally observed [5,7,8] and extensively studied in theory [6,12].

This work is motivated by the recent experimental realization of SO coupling in ultracold atomic gas [13–16]. We investigate the impact of SO coupling on Anderson localization of a spin-1/2 particle using the system of cold atomic gases trapped in a quasiperiodic one-dimensional (1D) optical lattice potential and simultaneously subject to the laser-induced SO interaction. A similar topic had also been addressed in Refs. [17,18], with the focus on the localization properties of relativistic Dirac particles with cold atoms in a light-induced gauge field. Our model and method are different from theirs and we do not consider the relativistic region.

The paper is organized as follows. Section II introduces the theoretical model and tight-binding approximation is applied in Sec. III. In Sec. IV we present the phase diagram and discuss its implications. Section V is devoted to the multifractal analysis of the atomic wave function, from which the proposed phase diagram is verified. The diffusion dynamics is studied in Sec. VI for an initially localized Gaussian wave packet. Finally we conclude in Sec. VII.

II. MODEL AND HAMILTONIAN

We consider the following model depicted in Fig. 1: cold atomic gas with internal spin states $|\uparrow\rangle$ and $|\downarrow\rangle$ confined in a spin-independent 1D quasiperiodic optical lattice potential $s_1 E_{R1}\sin^2(k_1 x)+s_2 E_{R1}\sin^2(k_2 x+\phi)$ along the x direction, which is formed by combining two incommensurate optical lattices together [5]. Here $k_i=2\pi/\lambda_i$ is the lattice wave number, s_i is the height of the lattice in units of the recoil energy $E_{R1}=h^2/2m\lambda_1^2$, and ϕ is the relative phase between the two standing-wave modes (without loss of generality, we assume $\phi=0$ in the following discussion). It is assumed that the depth of the lattice with wave vector k_1 is deep enough to serve as the tight-binding primary lattice. Meanwhile, a pair of counterpropagating Raman beams couple the atomic states $|\uparrow,k_x=q\rangle$ and $|\downarrow,k_x=q+2k_R\rangle$, which creates the effective SO coupling [13].

In the basis composed of atomic pseudospin states $\{|\uparrow\rangle,|\downarrow\rangle\}$, the single-particle Hamiltonian reads

$$\hat{h}=\left[\frac{p_x^2}{2m}+s_1E_{R1}\sin^2(k_1x)+s_2E_{R1}\sin^2(k_2x)\right]\hat{I}+\frac{\Omega}{2}\begin{pmatrix}0 & e^{2ik_Rx}\\ e^{-2ik_Rx} & 0\end{pmatrix},$$

with Ω the effective Raman coupling strength. Here we have assumed that the Raman two-photon detuning is 0. Then we introduce the dressed pseudospin states $\{|\uparrow\rangle'=|\uparrow\rangle e^{-ik_Rx},|\downarrow\rangle'=|\downarrow\rangle e^{ik_Rx}\}$, which is equivalent to performing a pseudospin rotation with the operator $\hat{R}(k_R)=\exp(-ik_Rx\hat{\sigma}_z)$, and perform a global pseudospin rotation $\hat{\sigma}_z\to\hat{\sigma}_y$, $\hat{\sigma}_y\to\hat{\sigma}_x$, $\hat{\sigma}_x\to\hat{\sigma}_z$ [13,16]. In the new basis, Hamiltonian $\hat{h}$ can then be rewritten

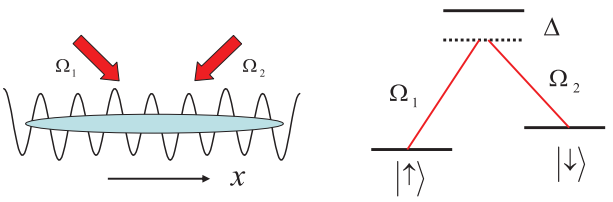

FIG. 1. (Color online) Schematic diagram showing the system under consideration.

as

$$\hat{h} = \hat{h}_{\rm SO} + V = \frac{(p_x - \hat{A})^2}{2m} + \frac{\Omega}{2}\hat{\sigma}_z + s_1 E_{R1}\sin^2(k_1 x) + s_2 E_{R1}\sin^2(k_2 x), \quad (1)$$

in which $\hat{h}_{\rm SO}$ describes single-particle motion in the presence of the effective SO coupling, which is embodied in the vector potential $\hat{A} = -m\lambda\hat{\sigma}_y$ ($\lambda = \hbar k_R/m$ characterizes spin-orbit coupling strength) and the effective Zeeman field $\Omega/2$.

$\hat{h}$ effectively describes a spin-1/2 particle moving in a 1D quasiperiodic potential and subject to both the Zeeman field and equal Rashba-Dresselhaus SO coupling, which can be used to simulate the corresponding condensed-matter system such as the motion of an electron in a one-dimensional semiconductor nanowire with disorder and SO interactions.

III. TIGHT-BINDING APPROXIMATION

In the language of quantum field theory, the total Hamiltonian describing our system reads

$$\hat{H}(x) = \int dx\, \hat{\Psi}^\dagger(x)\,\hat{h}(x)\,\hat{\Psi}(x), \quad (2)$$

with $\hat{\Psi} = (\hat{\psi}_\uparrow, \hat{\psi}_\downarrow)^T$ the atomic field operators.

In the tight-binding limit, the atomic field operator can be expanded as $\hat{\Psi}(x) = \sum_j w_j(x)\,\hat{c}_j$, where $w_j(x) = w(x - x_j)$ is the Wannier state of the primary lattice at the jth site and $\hat{c}_j = (\hat{c}_{j\uparrow}, \hat{c}_{j\downarrow})^T$ are annihilation operators. By considering that the tunneling takes place between nearest-neighbor sites and retaining only the on-site contribution of the secondary lattice, one can achieve the following description of Eq. (2) (with the energy measured in units of E_{R1} and length scaled in units of k_1^{-1}):

$$\begin{aligned}\hat{H} &= \sum_j \Big[-(\hat{c}_j^\dagger \hat{T}\hat{c}_{j+1} + \text{H.c.}) - \Delta\cos(2\pi\beta j)\,\hat{c}_j^\dagger\hat{c}_j + \frac{\Omega}{2}\hat{c}_j^\dagger\hat{\sigma}_z\hat{c}_j\Big] \\ &= \sum_j \Big\{-J[\hat{c}_j^\dagger(\cos\pi\gamma - i\hat{\sigma}_y\sin\pi\gamma)\hat{c}_{j+1} + \text{H.c.}] \\ &\quad - \Delta\cos(2\pi\beta j)\,\hat{c}_j^\dagger\hat{c}_j + \frac{\Omega}{2}\hat{c}_j^\dagger\hat{\sigma}_z\hat{c}_j\Big\},\end{aligned}$$

where the tunneling amplitude $\hat{T} = J\exp(-i/\hbar\int\hat{A}\,dl)$ is obtained through Peierls substitution [19,20], which was also used in recent works to study the impact of SO coupling on a two-dimensional Bose-Hubbard model [21–23]. $\int\hat{A}\,dl = \hat{A}(x_j - x_{j+1}) = \hbar\pi\gamma\hat{\sigma}_y$ is the integral of the vector potential along the hopping path with $\gamma = k_R/k_1$. J is the tunneling amplitude without SO coupling, $\beta = k_2/k_1$. J and Δ can be calculated as

$$J = -\int dx\, w_{j+1}(x)\left[-\frac{d^2}{dx^2} + s_1\sin^2 x\right]w_j(x),$$

$$\Delta = \frac{s_2\beta^2}{2}\int dx\,\cos(2\beta x)\,|w(x)|^2.$$

By writing $|\psi\rangle = \sum_{j,\sigma}\psi_{j,\sigma}\hat{c}_{j,\sigma}^\dagger|0\rangle$, the stationary Schrödinger equation $\hat{H}|\psi\rangle = E|\psi\rangle$ leads to

$$-J\cos(\pi\gamma)(\psi_{j+1,\uparrow} + \psi_{j-1,\uparrow}) - J\sin(\pi\gamma)(\psi_{j+1,\downarrow} - \psi_{j-1,\downarrow}) - \Delta\cos(2\pi\beta j)\psi_{j,\uparrow} + \frac{\Omega}{2}\psi_{j,\uparrow} = E\psi_{j,\uparrow}, \quad (3a)$$

$$-J\cos(\pi\gamma)(\psi_{j+1,\downarrow} + \psi_{j-1,\downarrow}) + J\sin(\pi\gamma)(\psi_{j+1,\uparrow} - \psi_{j-1,\uparrow}) - \Delta\cos(2\pi\beta j)\psi_{j,\downarrow} - \frac{\Omega}{2}\psi_{j,\downarrow} = E\psi_{j,\downarrow}. \quad (3b)$$

The second terms on the left-hand side of Eqs. (3), which are proportional to $J\sin(\pi\gamma)$, represent the spin-flipping tunneling which arises from the effective SO interaction. In the absence of SO coupling ($\gamma = 0, \Omega = 0$), spin-↑ and ↓ components are decoupled and we have

$$-J(\psi_{j+1} + \psi_{j-1}) - \Delta\cos(2\pi\beta j)\psi_j = E\psi_j, \quad (4)$$

which represents the typical Harper equation [24] or the Aubry-André model [25]. Equation (4) satisfies Aubry duality, as can be seen by performing the transformation $\psi_j = \sum_m\tilde{\psi}_m e^{im(2\pi\beta j)}$; inserting it into Eq. (4) will lead to

$$-\frac{\Delta}{2}(\tilde{\psi}_{m+1} + \tilde{\psi}_{m-1}) - 2J\cos(2\pi\beta m)\tilde{\psi}_m = E\tilde{\psi}_m. \quad (5)$$

Equations (4) and (5) are identical at $\Delta/J = 2$. Since the transformation made above represents the typical Fourier transform which transforms localized states to extended states and vice versa, then the critical point $\Delta/J = 2$ is identified as the transition point between the localized states and extended states, i.e., all the single-particle states are extended when $\Delta/J < 2$ and localized when $\Delta/J > 2$.

The properties of the Aubry-André model, as represented by Eq. (4), have been theoretically studied [26,27] and can be implemented in systems of Bloch electrons [20] and cold atoms [5]. We have also studied this model with Δ dressed by a cavity field through nonlinear feedback [9].

A similar transformation $\psi_{j,\sigma} = \epsilon_\sigma\sum_m\tilde{\psi}_{m,\sigma}e^{im(2\pi\beta j)}$ ($\epsilon_\uparrow = 1, \epsilon_\downarrow = i$) made to Eqs. (3) will lead to

$$-\frac{\Delta}{2}(\tilde{\psi}_{m+1,\uparrow} + \tilde{\psi}_{m-1,\uparrow}) + 2J\sin(\pi\gamma)\sin(2\pi\beta m)\tilde{\psi}_{m,\downarrow} - 2J\cos(\pi\gamma)\cos(2\pi\beta m)\tilde{\psi}_{m,\uparrow} + \frac{\Omega}{2}\tilde{\psi}_{m,\uparrow} = E\tilde{\psi}_{m,\uparrow}, \quad (6a)$$

$$-\frac{\Delta}{2}(\tilde{\psi}_{m+1,\downarrow} + \tilde{\psi}_{m-1,\downarrow}) + 2J\sin(\pi\gamma)\sin(2\pi\beta m)\tilde{\psi}_{m,\uparrow} - 2J\cos(\pi\gamma)\cos(2\pi\beta m)\tilde{\psi}_{m,\downarrow} - \frac{\Omega}{2}\tilde{\psi}_{m,\downarrow} = E\tilde{\psi}_{m,\downarrow}. \quad (6b)$$

A comparison between Eqs. (3) and (6) shows that the presence of the spin-flipping tunneling terms breaks the duality. This distinguishes our current work from that reported in Ref. [11], in which the authors studied a system of two-dimensional (2D) electrons on a square lattice subject to Rashba spin-orbit coupling and immersed in a perpendicular uniform magnetic field. In this system, it has been shown [11] that a generalized Aubry duality is preserved when tunneling along the two perpendicular lattice directions is exchanged. Such an operation is not available in our system as ours is an intrinsically 1D model.

Due to the lack of duality in the current model, it is not clear whether there exists a phase transition between the localized and extended states in the present system. In addition, what effect will SO coupling take? Will it enhance the tendency to localization or delocalization? We focus on these problems in the following discussion.

IV. PHASE DIAGRAM ANALYSIS

Here we follow the method in Ref. [11] to map the phase diagram using a quantity called the total width of all the energy bands B, which had been proved to be useful in investigating phase transition in a quasiperiodic system [11,26,27]. In order to observe its property, as people usually do, we first choose the optical lattice wavelength ratio β to be $\beta_n = F_n/F_{n+1} = p/q$, in which F_n is the nth Fibonacci number defined by the recursion relation $F_{n+1} = F_n + F_{n-1}$ with $F_0 = F_1 = 1$. When $n \to \infty$, $\beta_n \to (\sqrt{5}-1)/2$, which is the inverse of the golden ratio.

Since p and q are integers prime to each other, the system is periodic with the period q. Under the periodic boundary condition, according to Bloch's theorem, $\psi_{i+q,\sigma} = e^{ik_x q}\psi_{i,\sigma}$. Equations (3) then reduce to an eigenvalue problem $\mathcal{H}\psi = E\psi$ with $\psi = (\psi_{1,\uparrow},\psi_{1,\downarrow},\psi_{2,\uparrow},\psi_{2,\downarrow},\ldots,\psi_{q-1,\uparrow},\psi_{q-1,\downarrow},\psi_{q,\uparrow},\psi_{q,\downarrow})$ and the $2q \times 2q$ matrix $\mathcal{H}$ takes the following form:

$$\mathcal{H} = \begin{pmatrix} H_1 & L & 0 & \cdots & & 0 & e^{-ik_x q}L^\dagger \\ L^\dagger & H_2 & L & 0 & & & 0 \\ 0 & L^\dagger & H_3 & L & 0 & & \\ & 0 & \cdots & & & & \\ & & & & \cdots & L & 0 \\ 0 & & & 0 & L^\dagger & H_{q-1} & L \\ e^{ik_x q}L & 0 & & & 0 & L^\dagger & H_q \end{pmatrix}$$

with

$$H_j = \begin{pmatrix} -\Delta\cos(2\pi\beta j+\phi)+\frac{\Omega}{2} & 0 \\ 0 & -\Delta\cos(2\pi\beta j+\phi)-\frac{\Omega}{2} \end{pmatrix}$$

and

$$L = \begin{pmatrix} -J\cos(\pi\gamma) & -J\sin(\pi\gamma) \\ J\sin(\pi\gamma) & -J\cos(\pi\gamma) \end{pmatrix}.$$

The Hermite matrix $\mathcal{H}$ can be diagonalized with $2q$ real eigenvalues $E_i(k_x)$, which form $2q$ energy bands as the function of k_x in the first Brillouin zone $q|k_x| \leqslant \pi$.

In the absence of SO coupling, the energy bands are degenerate for spin-↑ and ↓, with the band edges located at $k_x = 0$ and $k_x = \pm\pi/q$, so B can be calculated by $B = \sum_{i=1}^{2q}|E_i(0) - E_i(\pm\pi/q)|$. It was first demonstrated in Ref. [26] that for extended states with $\Delta/J < 2$, B approaches a finite value for $q \to \infty$, while for localized states $\Delta/J > 2$, B rapidly tends to zero as $q \to \infty$, at the critical point $\Delta/J = 2$, $B \approx q^{-1}$. In this manner, the critical value $\Delta = \Delta_c$ signaling AL transition can be determined by observing the property of B as a function of the period q.

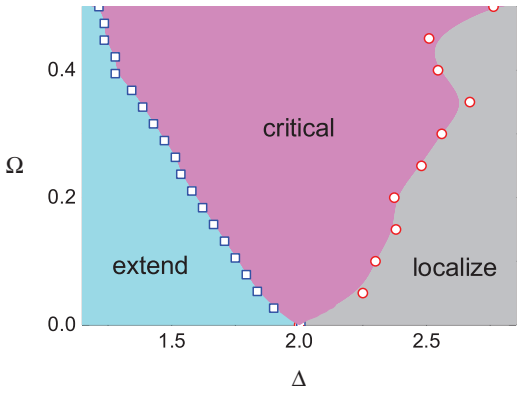

FIG. 2. (Color online) Phase diagram for Anderson localization of SO-coupled BEC in 1D quasiperiodic lattice in the parameter space Δ-Ω. $\gamma = 0.7$, Δ and Ω are estimated in units of J.

Now taking SO coupling into account, we anticipate that the phase diagram is composed of three different phases: (i) extended phase in which the energy spectrum is purely continuous and all the eigenstates are extended; (ii) localized phase is characterized by a purely dense point and all the wave functions are localized; and (iii) the energy spectrum is mixed in the critical phase with extended eigenstates coexisting with localized ones. Using the method described above, Δ_c is determined as a function of Ω, which is indicated in the phase diagram of Fig. 2 by the line separating the regions signaling localized phase and critical phase. Calculation is performed with the parameter of $\gamma = 0.7$, which is used throughout the paper and can be experimentally realized for ^{87}Rb atoms by adjusting the angle between Raman beams [13]. At $\Omega = 0$, AL transition occurs at $\Delta/J = 2$, reminiscent of the situation without SO coupling. This can be understood from Eq. (1) that SO interaction can be removed from the Hamiltonian through a unitary transformation with the operator $\hat{S} = \exp(-ix\hat{\sigma}_y/2\xi)$ when $\Omega = 0$. Examples of data are shown in Fig. 3(a). At $\Delta/J = 2.02$, B tends to zero for $\Omega < \Omega(\Delta_c)$ and B tends to a finite value for $\Omega > \Omega(\Delta_c)$.

Due to the fact that duality is broken by the SO coupling here, the boundary between extended phase and critical phase is not related to that which separates localized phase and critical phase, which is different from Ref. [11]. The extended phase and critical phase cannot be differentiated by examining the properties of B, since the energy spectrum contains absolutely continuous parts in both of these phases, which leads B to a finite value in the quasiperiodic limit, as shown in Fig. 3(b).

The localization property of the atomic wave function can be characterized with the inverse participation ratio (IPR) which is defined as

$$P^{-1} = \sum_{j=1}^{N}(|\psi_{j,\uparrow}|^4 + |\psi_{j,\downarrow}|^4),$$

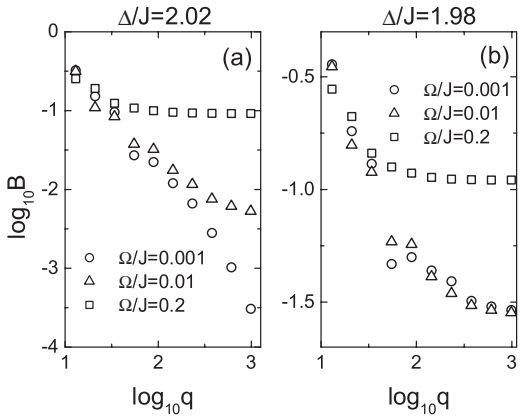

FIG. 3. Total bandwidth versus period q. At $q \to \infty$ the system becomes quasiperiodic. The parameters are specified in the figure.

in which N is the number of lattice sites and $\psi_{j,\uparrow(\downarrow)}$ are solutions of Eqs. (3) and fulfill the normalization condition $\sum_j(|\psi_{j,\uparrow}|^2 + |\psi_{j,\downarrow}|^2) = 1$. IPR reflects the inverse of the number of lattice sites being occupied by the atoms. For extended states, $P^{-1} \to 1/N$ and approach 0 for large N, while for localized states, IPR tends to a finite value and a larger value of P^{-1} means that the atoms are more localized in space.

We use IPR to determine the boundary separating the extended phase and critical phase, which is identified by the turning point of IPR as a function of Δ/J, as had been done in many previous works [9,12,28,29]. The calculation is performed with $\beta = F_{14}/F_{15} = 610/987$ and $N = F_{15} = 987$ under periodic boundary condition. This gives the extend-critical phase boundary shown in Fig. 2, which indicates that with the increase of the Rabi frequency Ω the system is more likely to start to become localized. In order to understand this, we plot the energy spectrum as a function of Δ/J. When Ω is relatively small, the spectrum shown in Fig. 4(a) possesses similar properties to that in the absence of SO coupling: Along with the increase of Δ/J, two major gaps divide the spectrum into three parts, each of which in turn divides into three smaller parts, and so on. This is because the value of $1/\beta$ lies between 2 and 3. The spectrum of localized states is then characterized by the presence of an infinite number of gaps and bands. The effective Zeeman term which is proportional to Ω, in combination with SO coupling and the lattice structure, takes the effect of opening gaps between different energy bands, as shown in Fig. 4(b). So the critical value Δ_c takes a smaller value with the increase of Ω.

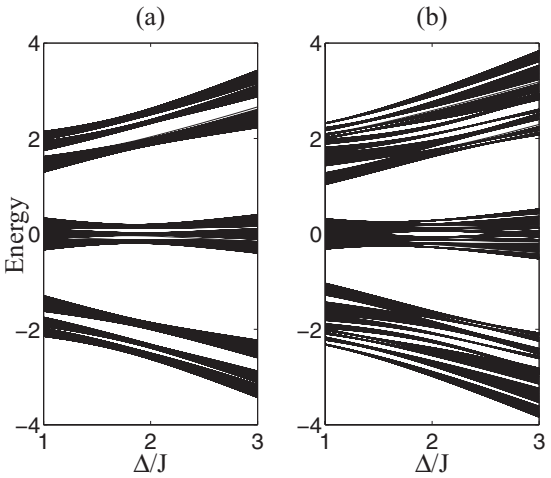

FIG. 4. Eigenenergies obtained from numerical diagonalization of Hamiltonian matrix, as a function of Δ/J. Calculations are performed under periodic condition with $\beta = 610/987$, $N = 987$, $\gamma = 0.7$ and (a) $\Omega = 0.1$; (b) $\Omega = 1$.

V. MULTIFRACTAL ANALYSIS OF WAVE FUNCTIONS

To check the proposed phase diagram, we investigate the scaling property of the wave functions using the method of multifractal analysis described in [11]. Taking the period of the lattice to be Fibonacci number F_n, from the wave functions $\{\psi_{j,\sigma}\}$ we have the probability $p_j = |\psi_{j,\uparrow}|^2 + |\psi_{j,\downarrow}|^2$, which is normalized as $\sum_{j=1}^{F_n} p_j = 1$. The scaling index α for p_j is defined as $p_j = F_n^{-\alpha}$. We then assume that the number of sites satisfying the scaling is proportional to $F_n^{f_n(\alpha)}$, and $f(\alpha)$ can be calculated as $f(\alpha) = \lim_{n\to\infty} f_n(\alpha)$.

The localization properties of wave functions are characterized by $f(\alpha)$ in the following manner: For extended wave functions, all the lattices satisfy $p_j \sim F_n^{-1}$, so $f(\alpha)$ is fixed at $f(\alpha = 1) = 1$. On the other hand, a localized wave function has a nonvanishing probability only on a finite number of sites. These sites have $\alpha = 0$ [$f(0) = 0$] and other sites with probability zero have $\alpha = \infty$ [$f(\infty) = 1$]. For critical wave functions, α has a distribution, which means that $f(\alpha)$ is a smooth function defined on a finite interval $[\alpha_{\min}, \alpha_{\max}]$.

Numerically we calculate $f_n(\alpha)$ for Fibonacci indices n and extrapolate them to $n \to \infty$. One can then discriminate extended, localized, and critical wave functions by examining the minimum value of α in the following manner:

$$\text{extended wave function } \alpha_{\min} = 1,$$
$$\text{critical wave function } \alpha_{\min} \neq 0, 1,$$
$$\text{localized wave function } \alpha_{\min} = 0.$$

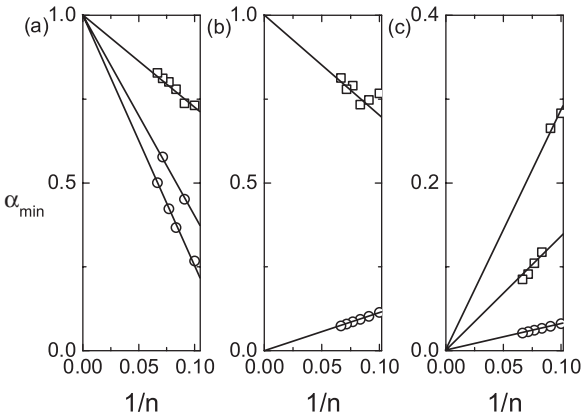

FIG. 5. $\alpha_{\min}$ versus $1/n$ for the wave functions of the lowest band ◯ ($i = 1$) and the center band □ ($i = F_n$). (a) $\Omega/J = 0.2$, $\Delta/J = 1.5$; (b) $\Omega/J = 0.4$, $\Delta/J = 1.5$; and (c) $\Omega/J = 2.5$, $\Delta/J = 0.1$ correspond to extend phase, critical phase, and localize phase, respectively.

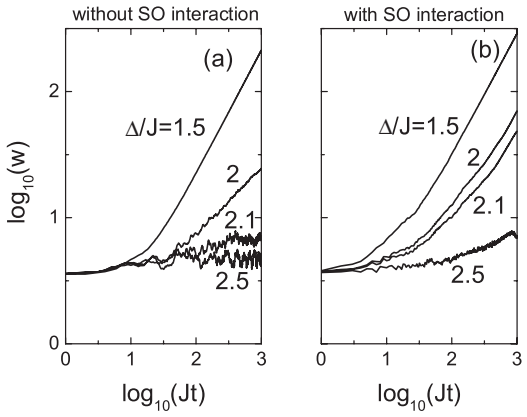

FIG. 6. Time evolution of the wave packet width $w(t)$: (a) without SO interaction; (b) in the presence of SO interaction with $\gamma = 0.7$ and $\Omega/J = 0.2$.

$\alpha_{\min}$ is calculated, for example, for wave functions and the results are shown in Fig. 5. The wave function of the lowest band is denoted by $i = 1$, while that at the center of the energy spectrum is denoted by $i = F_n$. First, for $\Omega/J = 0.2$, $\Delta/J = 1.5$ at which the system is in the extended phase according to the phase diagram in Fig. 2, $\alpha_{\min}$ extrapolates to 1 for both $i = 1$ and $i = F_n$, as shown in Fig. 5(a), indicating that the energy spectrum is purely continuous and all the wave functions are extended. The point $\Omega/J = 0.4$, $\Delta/J = 1.5$ corresponds to the critical phase in Fig. 2, and in Fig. 5(b) one can find that $\alpha_{\min}$ extrapolates to 0 for $i = 1$ and $\alpha_{\min}$ extrapolates to 1 for $i = F_n$. This suggests that the wave function at the edge of the energy spectrum is localized, while that at the center is extended, which indicates the existence of mobility edges.

The appearance of mobility edges here can be understood as the result of the breaking of original self-duality via SO interaction, which can also be aroused by other effects such as hopping beyond neighboring lattice sites [29,30]. We would like to note that, even if the duality is preserved, SO coupling can also lead to the appearance of critical phase and mobility edges, as had been demonstrated in [11].

VI. DIFFUSION DYNAMICS

In realistic experiment, localization properties can be investigated by loading the SO-coupled BEC into the quasiperiodic potential and observing its transportation along the lattice [5]. The equation of motion associated with Eqs. (3) is

$$i\frac{\partial \Psi_j}{\partial t} = -Je^{-i\pi\gamma\hat{\sigma}_y}(\Psi_{j+1} + \Psi_{j-1}) + \left[-\Delta\cos(2\pi\beta j) + \frac{\Omega}{2}\hat{\sigma}_z\right]\Psi_j, \tag{7}$$

where $\Psi_j = (\psi_{j,\uparrow}, \psi_{j,\downarrow})^T$. We study the diffusion of ultracold atomic gas in quasiperiodic optical lattice with Eq. (7) by taking the initial atomic wave function to be a localized Gaussian wave packet with width a,

$$\Psi_j(t=0) = (2a\sqrt{\pi})^{-1/2}e^{-j^2/2a^2}\begin{pmatrix}1\\ i\end{pmatrix},$$

in which we take $a = 5$ in the following calculation. Here we assume that the atomic wave packets initially lie in the center at

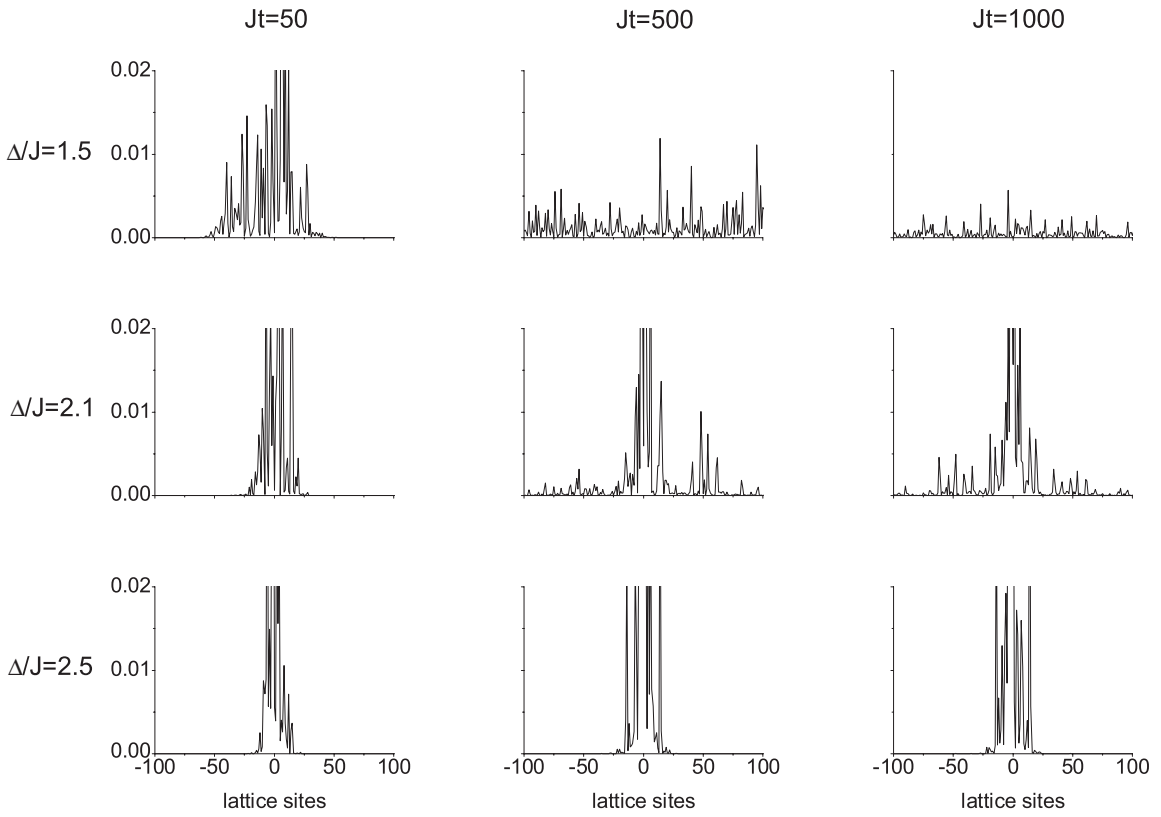

FIG. 7. Time evolution of wave packets $|\psi_{j,\uparrow}|^2$ corresponds to Fig. 6(b) at specific times.

$j = 0$ with the system size of 2000 lattice sites. The numerical simulation is performed with vanishing boundary condition and during the time evolution the atomic wave packet never reaches the boundaries so that the effect of boundary condition does not appear.

To measure the localization, we use the width of the wave packet defined as

$$w = \sqrt{\langle (\Delta x)^2 \rangle} = \left\{ \sum_j j^2 (|\psi_{j,\uparrow}|^2 + |\psi_{j,\downarrow}|^2) \right\}^{1/2}.$$

In the absence of SO coupling, the time evolution of $w(t)$ can be parametrized as $w(t) \sim t^\eta$ [6,31], and its property is intimately related to the localization properties of the system:

(i) In the extended phase of $\Delta/J < 2$, the wave packet will experience ballistic expansion with $\eta = 1$.

(ii) At the critical point of $\Delta/J = 2$ the wave packet is subject to subdiffusion with $\eta \sim 0.5$.

(iii) The wave packet is localized when $\Delta/J > 2$ and $\eta = 0$.

The above time-evolution properties are demonstrated in Fig. 6(a). In Fig. 6(b) we present the results in the presence of SO interaction. One can find that, for $\Delta/J = 2.1$, which corresponds to the critical phase shown in Fig. 2, the wave packet still subdiffuses with time evolution. In addition, the time evolution of the wave packet at sample time is shown in Fig. 7. At $\Delta/J = 1.5$ corresponding to the system in the extended phase, the wave packet rapidly diffuses and almost all the lattice sites become populated, while at $\Delta/J = 2.5$ for the localized phase of the system, there is no diffusion because in this regime the initial Gaussian wave packet can be decomposed into the superposition of several single-particle localized eigenstates. For the system in the critical phase at $\Delta/J = 2.1$, the wave-packet diffusion is accompanied with solitonlike structures in the center and spreading sideband, which reflects that extended and localized eigenstates coexist in the system.

Besides that, the nature of localized states can also be extracted from the momentum distribution of the atom stationary states. This is because a more localized atomic wave function corresponds to a wider momentum distribution via Fourier transformation. The momentum distribution can be measured by turning off the Raman lasers, releasing the atoms from the lattice, and performing time-of-flight imaging. Since our above discussions are for the dressed spin states $\{|\uparrow,k\rangle_d, |\downarrow,k\rangle_d\}$, their momentum distribution can be mapped from that of the bare spins $|\uparrow,k+k_R\rangle$ and $|\downarrow,k-k_R\rangle$ in the following manner:

$$|\uparrow,k\rangle_d = \frac{1+i}{2}|\uparrow,k+k_R\rangle + \frac{-1+i}{2}|\downarrow,k-k_R\rangle,$$
$$|\downarrow,k\rangle_d = \frac{1+i}{2}|\uparrow,k+k_R\rangle + \frac{1-i}{2}|\downarrow,k-k_R\rangle.$$

VII. CONCLUSION

In conclusion, we have studied the system of a SO-coupled spin-1/2 particle moving in a one-dimensional quasiperiodic potential. We mapped out the system phase diagram in the tight-binding regime and accordingly discussed the localization properties. In the absence of SO interaction the system can be mapped into the AA model and self-dual if $\Delta/J = 2$; SO interaction breaks the duality and leads to the appearance of critical phase, in which the extended and localized states coexist in the energy spectra. We also verified the phase diagram via multifractal analysis of the wave functions and diffusion dynamics of an initially localized Gaussian wave packet. Experimental detection of localization properties is discussed. We proposed an experimental realization of the system using cold atomic gas trapped in a quasiperiodic optical lattice potential and external laser fields. Since the two ingredients of our proposed scheme, the quasiperiodic optical lattice potential [5] and SO coupling [13,15,16], had already been achieved for cold atoms, it is expected that the localization properties discussed in this work can be readily observed in experiment.

ACKNOWLEDGMENTS

This work is supported by the National Basic Research Program of China (973 Program) under Grant No. 2011CB921604, the National Natural Science Foundation of China under Grants No. 11234003, No. 11129402, No. 11004057, and No. 10828408, the "Chen Guang" project supported by Shanghai Municipal Education Commission and Shanghai Education Development Foundation under Grant No. 10CG24, and sponsored by Shanghai Rising-Star Program under Grant No. 12QA1401000. H.P. is supported by the U.S. NSF, the Welch Foundation (Grant No. C-1669), and the DARPA OLE program.

[1] P. W. Anderson, Phys. Rev. **109**, 1492 (1958).

[2] T. Schwartz, G. Bartal, S. Fishman, and M. Segev, Nature (London) **446**, 52 (2006); Y. Lahini, A. Avidan, F. Pozzi, M. Sorel, R. Morandotti, D. N. Christodoulides, and Y. Silberberg, Phys. Rev. Lett. **100**, 013906 (2008); I. V. Shadrivov, K. Y. Bliokh, Y. P. Bliokh, V. Freilikher, and Y. S. Kivshar, *ibid.* **104**, 123902 (2010); J. Cheng and G. Huang, Phys. Rev. A **83**, 053847 (2011).

[3] L. Sanchez-Palencia, D. Clément, P. Lugan, P. Bouyer, G. V. Shlyapnikov, and A. Aspect, Phys. Rev. Lett. **98**, 210401 (2007).

[4] J. Billy, V. Josse, Z. Zuo, A. Bernard, B. Hambrecht, P. Lugan, D. Clément, L. Sanchez-Palencia, P. Bouyer, and A. Aspect, Nature (London) **453**, 891 (2008).

[5] G. Roati, C. D'Errico, L. Fallani, M. Fattori, C. Fort, M. Zaccanti, G. Modugno, M. Modugno, and M. Inguscio, Nature (London) **453**, 895 (2008).

[6] M. Larcher, F. Dalfovo, and M. Modugno, Phys. Rev. A **80**, 053606 (2009).

[7] B. Deissler, M. Zaccanti, G. Roati, C. D'Errico, M. Fattori, M. Modugno, G. Modugno, and M. Inguscio, Nat. Phys. **6**, 354 (2010).

[8] E. Lucioni, B. Deissler, L. Tanzi, G. Roati, M. Zaccanti, M. Modugno, M. Larcher, F. Dalfovo, M. Inguscio, and G. Modugno, Phys. Rev. Lett. **106**, 230403 (2011).
[9] L. Zhou, H. Pu, K. Zhang, X.-D. Zhao, and W. Zhang, Phys. Rev. A **84**, 043606 (2011).
[10] S. Hikami, A. I. Larkin, and Y. Nagaoka, Prog. Theor. Phys. **63**, 707 (1980).
[11] M. Kohmoto and D. Tobe, Phys. Rev. B **77**, 134204 (2008).
[12] M. Modugno, New J. Phys. **11**, 033023 (2009).
[13] Y.-J. Lin, K. Jimenez-Garcia, and I. B. Spielman, Nature (London) **471**, 83 (2011).
[14] For a review, see J. Dalibard, F. Gerbier, G. Juzeliūnas, and P. Öhberg, Rev. Mod. Phys. **83**, 1523 (2011), and references therein.
[15] P. Wang, Z.-Q. Yu, Z. Fu, J. Miao, L. Huang, S. Chai, H. Zhai, and J. Zhang, Phys. Rev. Lett. **109**, 095301 (2012).
[16] L. W. Cheuk, A. T. Sommer, Z. Hadzibabic, T. Yefsah, W. S. Bakr, and M. W. Zwierlein, Phys. Rev. Lett. **109**, 095302 (2012).
[17] S.-L. Zhu, D.-W. Zhang, and Z. D. Wang, Phys. Rev. Lett. **102**, 210403 (2009).
[18] M. J. Edmonds, J. Otterbach, R. G. Unanyan, M. Fleischhauer, M. Titov, and P. Öhberg, New J. Phys. **14**, 073056 (2012).
[19] R. E. Peierls, Z. Phys. **80**, 763 (1933).
[20] D. R. Hofstadter, Phys. Rev. B **14**, 2239 (1976).
[21] K. Osterloh, M. Baig, L. Santos, P. Zoller, and M. Lewenstein, Phys. Rev. Lett. **95**, 010403 (2005).
[22] W. S. Cole, S. Zhang, A. Paramekanti, and N. Trivedi, Phys. Rev. Lett. **109**, 085302 (2012).
[23] J. Radić, A. Di Ciolo, K. Sun, and V. Galitski, Phys. Rev. Lett. **109**, 085303 (2012).
[24] P. G. Harper, Proc. Phys. Soc. London, Ser. A **68**, 874 (1955).
[25] S. Aubry and G. André, Ann. Isr. Phys. Soc. **3**, 33 (1980).
[26] M. Kohmoto, Phys. Rev. Lett. **51**, 1198 (1983).
[27] D. J. Thouless, Phys. Rev. B **28**, 4272 (1983).
[28] G. Dufour and G. Orso, Phys. Rev. Lett. **109**, 155306 (2012).
[29] J. Biddle and S. Das Sarma, Phys. Rev. Lett. **104**, 070601 (2010).
[30] D. J. Boers, B. Goedeke, D. Hinrichs, and M. Holthaus, Phys. Rev. A **75**, 063404 (2007).
[31] H. Hiramoto and S. Abe, J. Phys. Soc. Jpn. **57**, 1365 (1988).